Sensorless enhancement of an atomic force microscope micro-cantilever quality factor using piezoelectric shunt control

M. Fairbairn[a] and S. O. R. Moheimani[b]
School of Electrical Engineering and Computer Science, The University of Newcastle, Callaghan, NSW 2308, Australia

(Received 10 January 2013; accepted 1 May 2013; published online 23 May 2013)

The image quality and resolution of the Atomic Force Microscope (AFM) operating in tapping mode is dependent on the quality (Q) factor of the sensing micro-cantilever. Increasing the cantilever Q factor improves image resolution and reduces the risk of sample and cantilever damage. Active piezoelectric shunt control is introduced in this work as a new technique for modifying the Q factor of a piezoelectric self-actuating AFM micro-cantilever. An active impedance is placed in series with the tip oscillation voltage source to modify the mechanical dynamics of the cantilever. The benefit of using this control technique is that it removes the optical displacement sensor from the Q control feedback loop to reduce measurement noise in the loop and allows for a reduction in instrument size.
 [http://dx.doi.org/10.1063/1.4805108]

I. INTRODUCTION

The Atomic Force Microscope (AFM)[1] obtains three-dimensional images of sample surfaces through measurement of the interatomic forces between a sharp probe tip, located at the end of a micro-cantilever, and the sample surface. When operating in tapping mode[2] the cantilever tip is oscillated at or close to its first resonance frequency, lightly touching the sample once every oscillation cycle. A schematic showing the typical instrumentation of an AFM operating in tapping mode is shown in Fig. 1.

The sample is placed on a piezoelectric scanner which scans the sample in a raster pattern below the cantilever. As the sample is scanned below the cantilever the cantilever tip oscillation amplitude $A(t)$ varies in proportion to the sample topography. Cantilever deflection is measured optically.[3,4]

A feedback controller regulates the vertical position of the sample, maintaining $A(t)$ at a set-point value A_{set}. As the sample topography is an input disturbance to this feedback loop the output of the controller is proportional to variations in the sample topography. A three-dimensional image of the sample is obtained by plotting the control signal as a function of the lateral scan position.

The variation in $A(t)$ as a result of a change in sample height is dependent on the cantilever Q factor. A high Q factor cantilever produces a larger change in $A(t)$ than a low Q factor cantilever. The high Q factor cantilever, therefore, has a higher force sensitivity[5–7] providing better image resolution. For samples which have very fine features it is beneficial to use a high Q factor cantilever for high resolution images. Biological samples are commonly imaged in a liquid environment. Hydrodynamic forces cause a significant reduction of the cantilever Q factor[8,9] when imaging in liquid. This reduction in cantilever Q factor reduces the force sensitivity of the cantilever considerably.

It is important to minimize tip-sample forces in order to minimize tip/sample damage and deformation of soft samples. The tip-sample force is inversely proportional to the cantilever Q factor.[9,10] The reduction in sample deformation, as a result of increasing the cantilever Q factor, has been demonstrated by several authors.[11–13]

The cantilever Q factor may be modified by feedback of the cantilever tip velocity.[14] This is termed active Q control. It is difficult and relatively expensive to incorporate a velocity sensor into the AFM. Therefore, it is necessary to estimate tip velocity from the displacement signal. Differentiation of the displacement signal is not recommended as high frequency noise is amplified in the feedback loop. Tip velocity is commonly estimated by delaying the displacement signal by $\frac{3\pi}{2}$ radians at the tip oscillation frequency. A gain is then applied to this signal and subtracted from the probe oscillation signal to obtain the desired cantilever Q factor.

One drawback of using the time delay method of velocity estimation is that spill-over effects from the control action may affect higher order modes of the cantilever, leading to possible degradation of system performance.[15]

The feedback signal used for most implementations of active Q control relies on the displacement signal obtained from the optical sensor. The optical deflection sensing technique used to measure cantilever tip displacement in commercial AFMs introduces a significant amount of noise into the deflection measurement. In addition to electronic noise, two other forms of noise are introduced by the optical sensor. The first form of noise introduced by the optical sensor is due to stray beams of light reflecting off the sample surface and back into the sensor.[16] The second form of noise is due to light reflecting back from the cantilever and the sample into the laser source.[16] Imaging in a liquid environment is particularly problematic due to reflection and refraction of the laser beam at the interface between air and water.

Other problems with the optical deflection sensing technique include the time taken to align the laser beam and the size of the sensor. The task of aligning the laser beam must be

[a]Electronic mail: Matthew.Fairbairn@newcastle.edu.au
[b]Electronic mail: Reza.Moheimani@newcastle.edu.au

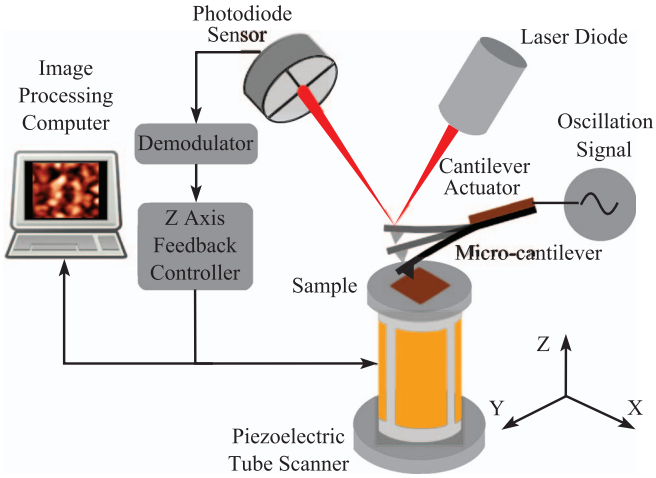

FIG. 1. Tapping mode AFM instrumentation.

completed every time that the cantilever is changed. This can be a tedious and time consuming task. The optical sensor occupies a relatively large amount of space. Reducing the size of the sensor is an advantage for applications which use an array of cantilevers[17–19] and to reduce the size of the AFM.[18]

The technique of active piezoelectric shunt control, introduced in this work to modify the effective Q factor of a piezoelectric self-actuated AFM micro-cantilever, removes the optical sensor from the Q control feedback loop. If the cantilever displacement can be measured with the piezoelectric transducer[20–22] it would be possible to remove the optical sensor from the AFM altogether, overcoming the limitations of the optical sensing technique mentioned above.

II. ACTIVE PIEZOELECTRIC SHUNT CONTROL

Passive piezoelectric shunt control[23] is a popular method of controlling vibration in structures such as spacecraft[24] and aircraft components.[25] A piezoelectric transducer is bonded to the surface of the structure with a passive electrical impedance connected to its electrodes. The piezoelectric transducer converts the mechanical energy of the structure to electrical energy and vice versa. The dynamics of the electrical circuit have a strong influence on the mechanical dynamics of the structure.

Fairbairn *et al.*[26] reduced the Q factor of a piezoelectrically actuated AFM micro-cantilever using passive piezoelectric shunt control. A synthetic impedance emulating an inductance and a resistance was placed in series with the cantilever oscillation voltage source to create an *LRC* circuit. This *LRC* circuit was tuned to the mechanical resonance of the cantilever to ensure that the electrical dynamics of the circuit had maximum influence over the mechanical dynamics of the cantilever. By tuning the resistance in the circuit a reduction in the cantilever Q factor from 297.6 to 35.5 was achieved.

Passive piezoelectric shunt control cannot be used in applications where an increase in the cantilever Q factor is required to increase force sensitivity and reduce tapping forces. To increase the cantilever Q factor using piezoelectric shunt control, energy must be added to the system. This requires the design of an active impedance in the piezoelectric shunt control framework.

The concept of using active piezoelectric shunt control to increase the Q factor of a cantilever has recently been demonstrated by Zhao *et al.*[27] Their experiments were conducted on a large cantilever (0.043 m × 0.433 m) with a resonance frequency of 91.7 Hz. An inductance and a negative resistance were connected to the terminals of a piezoelectric transducer which was bonded to the cantilever surface. To test the influence of the electrical impedance on the cantilever dynamics a separate piezoelectric transducer bonded to the cantilever was used for actuation.

In this work the technique of active piezoelectric shunt control is applied to a piezoelectric AFM micro-cantilever with a resonance frequency of approximately 50 kHz. The piezoelectric layer on the surface of the cantilever is used to simultaneously oscillate the cantilever and modify its dynamics in a way that enhances the Q factor.

A. Piezoelectric transducer electrical model

The AFM micro-cantilever chosen to demonstrate the concept of active piezoelectric shunt control in this work is the DMASP micro-cantilever manufactured by Bruker.[28] This device consists of a silicon cantilever which has a length of 120 μm and a width of 55 μm with a thin layer of piezoelectric zinc-oxide (ZnO) material deposited on the bottom surface. A probe tip which has a height of 15–20 μm and a tip radius of approximately 10 nm is found on the underside of the cantilever. A layer of titanium gold (Ti/Au) is bonded above and below the ZnO layer acting as electrodes. Applying a voltage to the electrodes causes the piezoelectric layer to expand or contract, depending on the polarity of the voltage, resulting in flexure of the cantilever. A sinusoidal voltage is applied to the electrodes to oscillate the cantilever tip when operating in tapping mode.

In the design of piezoelectric shunt control systems the piezoelectric transducer is commonly modeled electrically as a strain dependent voltage source v_p in series with a capacitance C_p.[23] This model was used to design the passive piezoelectric shunt control system used for reduction of the cantilever Q factor in Ref. 26.

Initial experiments with active piezoelectric shunt control of the DMASP micro-cantilever for Q factor enhancement indicated that the v_p in series with C_p model does not work well for this application. The experimental results did not match the values calculated for the shunt impedance parameters. This issue was also observed by Zhao *et al.*[27] in their experimental work. Zhao *et al.*[27] concluded that the mismatch between expected results and experimental results was due to frequency dependent electrical energy losses (dielectric losses) which may be modeled as a resistance R_p in parallel with C_p and v_p.

The frequency response of the DMASP micro-cantilever electrical impedance was measured in Refs. 29–31. Significant electrical energy losses in the ZnO piezoelectric transducer were observed.

When the cantilever is modeled electrically as a resistance R_p in parallel with C_p and v_p the transfer function from a voltage $v(s)$ applied to the transducer terminals to the charge $q(s)$ generated at the terminals is represented by

$$G_{qv}(s) = \frac{q(s)}{v(s)} = \alpha C_p G_{dv}(s) + C_p + \frac{1}{R_p s}, \tag{1}$$

where G_{dv} is the transfer function from $v(s)$ to the cantilever tip displacement $d(s)$ and is given by

$$G_{dv}(s) = \frac{d(s)}{v(s)} = \frac{\beta_v \omega_n^2}{s^2 + \frac{\omega_n}{Q} s + \omega_n^2}. \tag{2}$$

Here ω_n is the natural frequency of the cantilever, β_v is the steady state gain of G_{dv}, and α is the piezoelectric voltage-displacement coefficient ($\alpha = \frac{v_p}{d}$).

The impedance of the piezoelectric transducer may now be derived as

$$\begin{aligned} Z_p(s) &= \frac{v(s)}{i(s)} = \frac{v(s)}{sq(s)} \\ &= \frac{1}{sG_{qv}(s)} = \frac{1}{\alpha C_p G_{dv}(s) s + C_p s + \frac{1}{R_p}}. \end{aligned} \tag{3}$$

The values for C_p and R_p were measured using an Agilent E4980A *LCR* meter. C_p was measured to be 28.5 pF and R_p was found to be 6.7 MΩ.

The frequency response of $G_{dv}(s)$ was obtained by applying a pseudo random signal to the cantilever electrodes and measuring the resulting tip displacement with a Microscope Scanning Laser Doppler Vibrometer (Polytec MSV 400). The frequency response of $G_{dv}(s)$ is shown in Fig. 2. The mathematical model of $G_{dv}(s)$ obtained by system identification is

$$G_{dv}(s) = \frac{2126}{s^2 + 1472s + 1.119 \times 10^{11}} \tag{4}$$

and is also shown in Fig. 2.

A frequency response of the cantilever impedance, shown in Fig. 3, was obtained by measuring the voltage appearing across its electrodes in response to the application of a swept sine current. The transfer function obtained from this

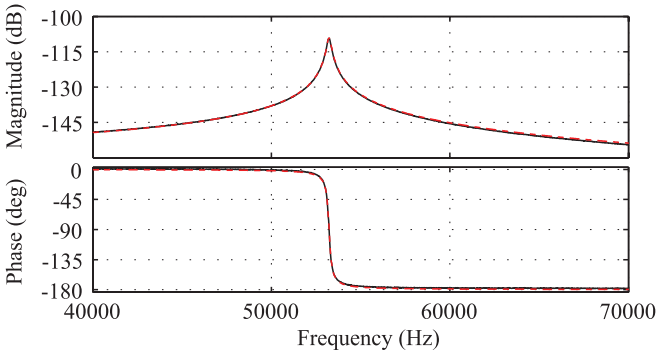

FIG. 2. DMASP micro-cantilever frequency response (- -) and fitted model (—).

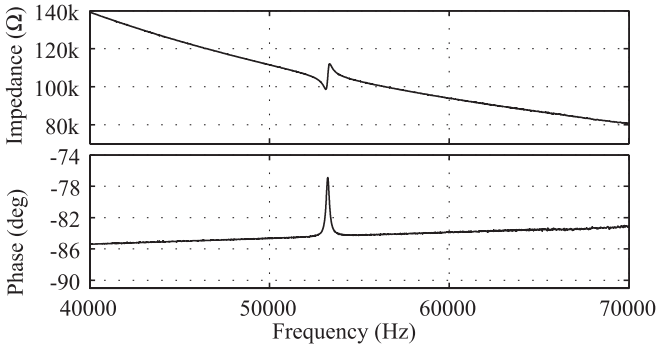

FIG. 3. Frequency response of the DMASP micro-cantilever electrical impedance.

frequency response is

$$Z_p(s) = \frac{s^2 + 1472s + 1.119 \times 10^{11}}{2.85 \times 10^{11} s^3 + 1.912 \times 10^7 s^2 + 3.191s + 16700}. \tag{5}$$

By equating (3) and (5) the value of α was found to be approximately 4×10^4 V/m.

B. Electromechanical model of the piezoelectric shunt system

A schematic of the micro-cantilever with the attached shunt circuit is shown in Fig. 4. The piezoelectric shunt control system may be modeled by the block diagram of Fig. 5. In this representation the cantilever is modeled as the system G. The cantilever has two inputs: the terminal voltage v and a disturbance strain w. This disturbance strain is a result of variations in the sample topography when scanning. The cantilever's two outputs are the tip displacement d and the charge generated at its terminals q. v_s is the voltage applied to the circuit and v_z is the voltage appearing across the terminals of the shunt impedance. The initial tip displacement due to a disturbance is represented by d_w. The transfer function from $w(s)$ to $d_w(s)$ is

$$G_{d_w w}(s) = \frac{d_w(s)}{w(s)} = \frac{\beta_w \omega_n^2}{s^2 + \frac{\omega_n}{Q} s + \omega_n^2}, \tag{6}$$

where β_w is the steady state gain of $G_{d_w w}(s)$.

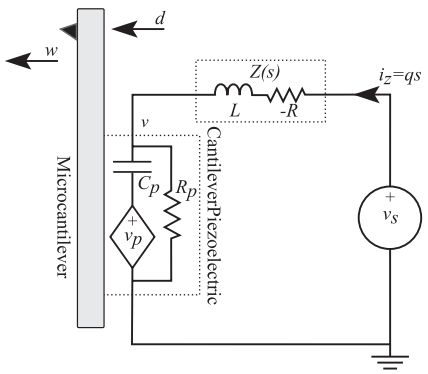

FIG. 4. Piezoelectric AFM micro-cantilever with attached shunt circuit.

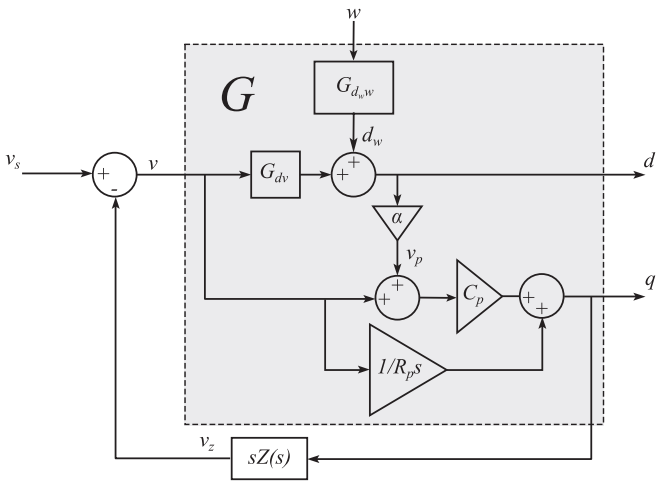

FIG. 5. Block diagram of the piezoelectric shunt control system.

C. Modelling the transfer function from actuating voltage to tip displacement

From the block diagram of Fig. 5 the transfer function from v_s to v may be derived as

$$G_{vv_s}(s) = \frac{v(s)}{v_s(s)} = \frac{1}{1 + sZ(s)G_{qv}(s)}. \tag{7}$$

Substituting (1) into (7) gives

$$G_{vv_s}(s) = \frac{\frac{1}{1+sZ(s)\left(C_p+\frac{1}{R_p s}\right)}}{1 + \frac{sZ(s)C_p\alpha G_{dv}(s)}{1+sZ(s)\left(C_p+\frac{1}{R_p s}\right)}}. \tag{8}$$

Let

$$H(s) = \frac{1}{1 + sZ(s)\left(C_p + \frac{1}{R_p s}\right)} \tag{9}$$

and

$$K(s) = \frac{sZ(s)C_p\alpha}{1 + sZ(s)\left(C_p + \frac{1}{R_p s}\right)}, \tag{10}$$

then

$$G_{vv_s}(s) = \frac{H(s)}{1 + K(s)G_{dv}(s)}. \tag{11}$$

The transfer function from v_s to d, when the shunt impedance is connected, is now found to be

$$G_{dv_s}(s) = G_{vv_s}(s)G_{dv}(s) = \frac{H(s)G_{dv}(s)}{1 + K(s)G_{dv}(s)}. \tag{12}$$

G_{dv_s} may be viewed as a negative feedback loop with a filter $H(s)$ in the feed forward path.

When imaging in tapping mode the oscillation voltage is a sinusoidal signal. The filter $H(s)$ results in a modification in the magnitude and phase of this signal. The modification of phase does not affect the performance of the device and the modification in the magnitude may be accommodated for by varying the amplitude of the input signal.

D. Modelling the transfer function from sample topography to tip displacement

To obtain the transfer function from $w(s)$ to $d(s)$, $v_s(s)$ is first set to zero. From Fig. 5 it is observed that

$$v(s) = -v_z(s) \tag{13}$$

and

$$v_z(s) = sq(s)Z(s), \tag{14}$$

where $q(s)$ is given by

$$q(s) = -v_z(s)C_p - v_z(s)\alpha C_p G_{dv}(s) - \frac{v_z(s)}{R_p s} + d_w(s)\alpha C_p. \tag{15}$$

Substituting (15) into (14) gives

$$v_z(s) = (-v_z(s)C_p - v_z(s)\alpha C_p G_{dv}(s) - \frac{v_z(s)}{R_p s} + d_w(s)\alpha C_p)sZ(s). \tag{16}$$

Substituting (13) into (16) results in the transfer function

$$G_{vd_w}(s) = \frac{v(s)}{d_w(s)} = \frac{-\alpha s Z(s)C_p}{1 + sZ(s)\left(C_p + \frac{1}{R_p s}\right) + \alpha s Z(s)C_p G_{dv}(s)}. \tag{17}$$

From Fig. 5 it is observed that

$$d(s) = G_{vd_w}(s)G_{dv}(s)d_w(s) + d_w(s). \tag{18}$$

Substituting (17) into (18) results in the transfer function

$$G_{dd_w}(s) = \frac{d(s)}{d_w(s)} = \frac{1}{1 + \frac{\alpha s Z(s)C_p G_{dv}(s)}{1+sZ(s)\left(C_p+\frac{1}{R_p s}\right)}} = \frac{1}{1 + K(s)G_{dv}(s)}. \tag{19}$$

Combining (19) and (6) results in the transfer function

$$G_{dw}(s) = G_{dd_w}(s)G_{d_w w}(s) = \frac{G_{d_w w}(s)}{1 + K(s)G_{dv}(s)}. \tag{20}$$

$G_{d_w w}(s)$ has the same poles as $G_{dv}(s)$, the only difference being the steady state gain β_w. The transfer function $G_{dw}(s)$ may be written as

$$G_{dw}(s) = \frac{\lambda G_{dv}(s)}{1 + K(s)G_{dv}(s)}, \tag{21}$$

where $\lambda = \frac{\beta_w}{\beta_v}$. In the above form $G_{dw}(s)$ may be viewed as a negative feedback loop, as shown in Fig. 6. The closed loop poles may be placed in the s plane to obtain the desired Q factor by design of the feedback controller $K(s)$.

Note that the transfer function of the controller $K(s)$, when an impedance $Z(s) = Ls - R$ is applied, is a filter with a phase lag of $\frac{\pi}{2}$ at the filters resonance frequency f_r. If f_r is tuned to the oscillation frequency of the cantilever the controller is effectively estimating the cantilever tip velocity and applying a negative gain. The gain and bandwidth of control may be tuned by varying the parameters R and L.

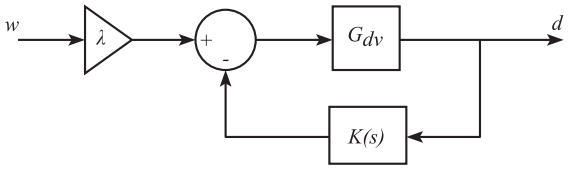

FIG. 6. Feedback interpretation of the transfer function from a disturbance w to tip displacement d.

III. SYNTHETIC IMPEDANCE

An active impedance such as $Ls - R$ cannot be implemented using passive components. Cantilever parameters, such as C_p and α, will vary with material imperfections and manufacturing tolerances. Environmental conditions such as humidity, temperature, and air pressure will cause variations in the cantilever resonance frequency. The values of R and L required to obtain a desired cantilever Q factor will, therefore, vary from cantilever to cantilever and with environmental conditions. A synthetic impedance was designed to implement the active impedance and to allow for fine tuning of the values of R and L.

To implement an arbitrary impedance $Z(s)$ synthetically[32] the terminal voltage $v_z(s)$ is measured and a current source applies an appropriate current to mimic the voltage to current relationship of the impedance ($Z(s) = \frac{v_z(s)}{i_z(s)}$). The current supplied by the current source is $i_z(s) = v_z(s)Y(s)$, where $Y(s) = \frac{1}{Z(s)}$.

The circuit of Fig. 7, which shows the piezoelectric micro-cantilever attached to a synthetic impedance, is equivalent to the shunt impedance circuit shown in Fig. 4 if

$$F_Y(s) = \frac{R}{Y(s)} = \frac{R}{Ls - R}. \tag{22}$$

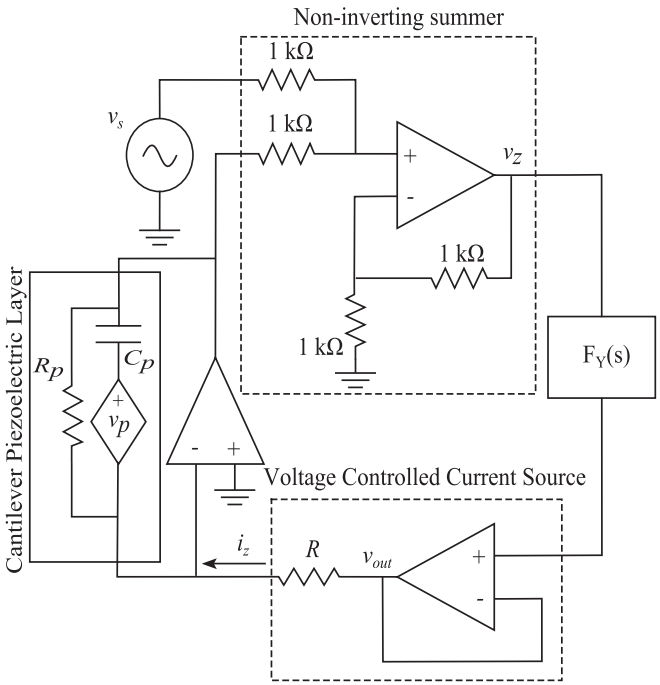

FIG. 7. Piezoelectric shunt control circuit implemented with a synthetic impedance.

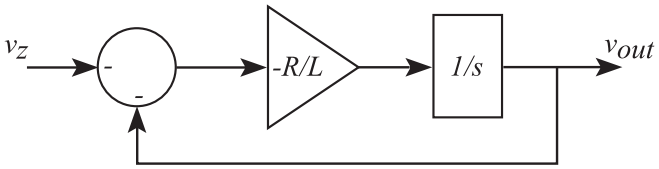

FIG. 8. Admittance filter $F_Y(s)$.

From Fig. 7 it is observed that

$$\frac{v_{out}(s)}{v_z(s)} = F_Y(s) = \frac{R}{Ls - R} \tag{23}$$

and

$$i_z(s) = \frac{v_{out}(s)}{R}. \tag{24}$$

The resulting impedance is now found to be

$$Z(s) = \frac{v_z(s)}{i_z(s)} = \frac{v_z(s)R}{v_{out}(s)} = Ls - R. \tag{25}$$

A block diagram implementation of $F_Y(s)$ is shown in Fig. 8. By varying R and the gain ($\frac{R}{L}$) of the integrator in the filter $F_Y(s)$ the values of L and R may be modified accordingly.

The admittance filter $F_Y(s)$ is implemented with operational amplifiers in the schematic of Fig. 9 which shows the piezoelectric micro-cantilever attached to the synthetic impedance. The non-inverting summer, shown in Fig. 7, which adds the oscillation voltage v_s to the cantilever terminal voltage is incorporated into the admittance filter circuit to reduce the number of operational amplifiers required in the circuit. The operational amplifiers used in this circuit are Linear Technology LT1468 operational amplifiers.[33] In this implementation the value of the inductance is determined by $L = RR_IC$.

When increasing the cantilever Q factor the poles of the cantilever are pushed toward the $j\omega$ axis of the complex plane. As the poles are shifted toward the $j\omega$ axis the risk of the cantilever becoming unstable is increased. Cantilever instability may result in damage to the cantilever and/or sample. The maximum amplitude at which the cantilever can oscillate, if the system goes unstable, may be controlled by limiting the power supply voltage of the operational amplifier to which the cantilever is connected, in Fig. 9. This may avoid any damage which might occur if the system does become unstable.

IV. EXPERIMENTAL DEMONSTRATION

A. Determination of shunt impedance parameters

1. Inductance

For the electrical dynamics to have a sufficient influence on the mechanical dynamics of the cantilever the resonance frequency f_e created by the electrical circuit must be tuned close to the mechanical resonance f_r of the cantilever. The inductance tuning ratio is defined as

$$\delta = \frac{f_e}{f_r}. \tag{26}$$

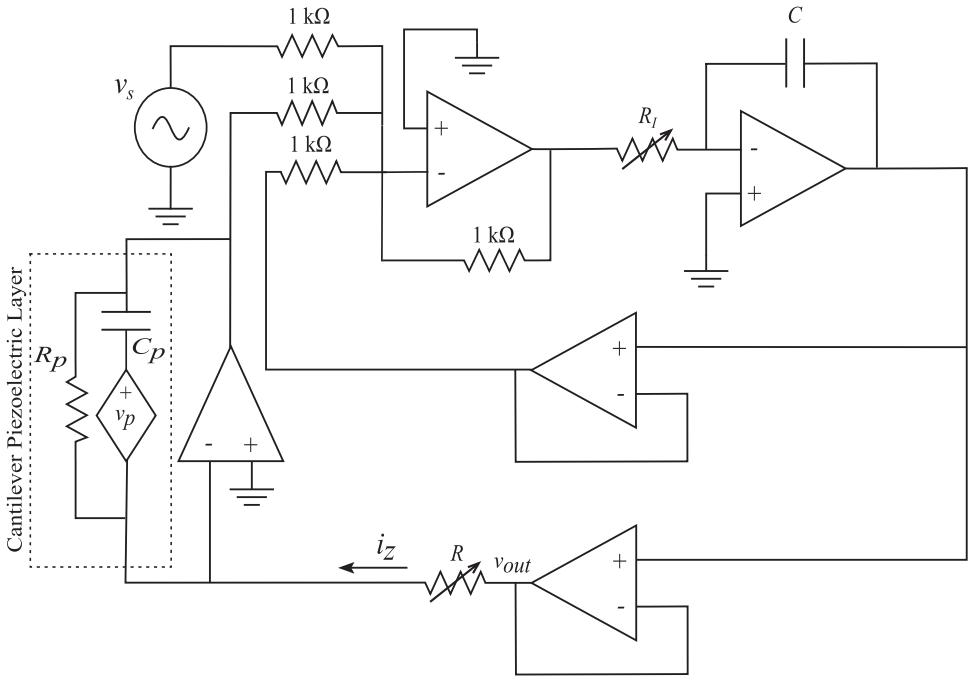

FIG. 9. Piezoelectric shunt control circuit implemented with a synthetic impedance. In this schematic the admittance filter $F_Y(s)$ is implemented with operational amplifiers.

For the piezoelectric shunt control circuit shown in Fig. 4 f_e is given by

$$f_e = \frac{1}{2\pi}\sqrt{\frac{1}{LC_p} - \frac{1}{(R_pC_p)^2}}. \tag{27}$$

The necessary inductance may be found by tuning δ close to 1. For an initial demonstration of the active piezoelectric shunt control technique this was achieved by setting $f_e = f_r$ ($\delta = 1$). f_r was measured from the frequency response shown in Fig. 2 to be 53234 Hz, therefore f_e was be tuned to 53234 Hz. The necessary inductance is calculated by substituting the values for f_e, C_p, and R_p into (27). The value for L was found to be 313.56 mH.

2. Resistance

The characteristic equation (A_{CL}) of $G_{dw}(s)$ is $1 + K(s)G_{dv}$. A root locus of $G_{dw}(s)$ was obtained by rearranging A_{CL} into the form

$$A_{CL} = 1 + R\frac{(\psi s^3 + \psi 2\zeta\omega_r s^2 + \psi\omega_r^2 s + C_p\alpha\beta_v\omega_r^2 s)}{L\psi s^4 + L\psi 2\zeta\omega_r s^3 + \gamma s^2 + 2\zeta\omega_r s + \omega_r^2}, \tag{28}$$

where $\psi = C_p + \frac{1}{R_p s}$ and $\gamma = 1 + L\psi\omega_r^2 + LC_p\alpha\beta_v\omega_r^2$.

The root locus when δ is tuned to 1, for $R \in [-\infty, 0]$, is shown in Fig. 10. A zoomed in view of the upper left quadrant of the root locus is shown in Fig. 11. As R is reduced, the poles of $G_{dw}(s)$ shift toward the right of the complex plane, increasing the Q factor of the cantilever. The cantilever reaches a point of instability when the poles cross the imaginary axis. The value of R, which causes the system to go unstable, is determined by conducting a Routh-Hurwitz stability analysis on A_{CL}. The value of R which causes system instability, when δ is tuned to 1, is $-3250\ \Omega$. A slightly higher value of resistance ($-3150\ \Omega$) was chosen for this initial test to ensure stability of the cantilever.

B. Cantilever frequency response

The force sensitivity and tip-sample force of the AFM operating in tapping mode are dependent on the dynamics of $G_{dw}(s)$. To measure the frequency response of $G_{dw}(s)$ a piezoelectric actuator is placed underneath the cantilever mounting base with an excitation signal applied to the actuator. Difficulties were encountered with this method due to

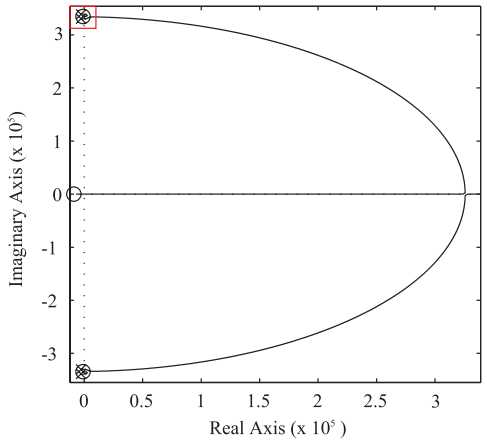

FIG. 10. Root locus of $G_{dw}(s)$ when $\delta = 1$. A zoomed in view of the section inside the red square is shown in Fig. 11.

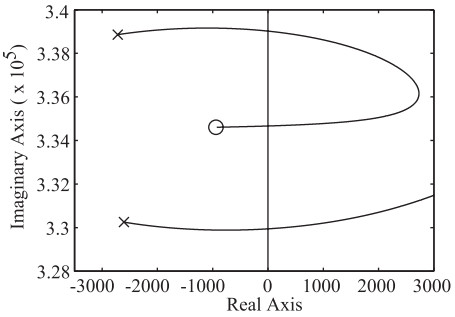

FIG. 11. Upper left quadrant of the root locus of $G_{dw}(s)$ when $\delta = 1$ ($R \in [-\infty, 0]$).

the additional dynamics added to the system by the cantilever mounting base and the piezoelectric actuator.

An alternative method of measuring the frequency response of $G_{dw}(s)$, when the active piezoelectric shunt controller is implemented, is to apply a filtered excitation signal to the cantilever electrodes. Equating (12) and (21) gives

$$G_{dw}(s) = \lambda H^{-1}(s) G_{dv_s}(s). \tag{29}$$

$G_{dw}(s)$ is therefore equivalent to $H^{-1}(s)G_{dv_s}(s)$ multiplied by a gain λ. The poles of the system are not affected by the gain λ. λ may therefore be disregarded and the frequency response of $H^{-1}(s)G_{dv_s}(s)$ used to determine the Q factor of $G_{dw}(s)$. The filter $H^{-1}(s)$ is non-causal. $H^{-1}(s)$ may be approximated physically by adding fast poles into the transfer function. The approach taken in this work was to obtain the frequency response of $H^{-1}(s)G_{dv_s}(s)$ by filtering the frequency response of $G_{dv_s}(s)$ with $H^{-1}(s)$ afterward using MATLAB.

An active shunt impedance containing a negative resistance of $-3150\ \Omega$ and an inductance of 313.56 mH was applied to the DMASP micro-cantilever. The frequency response plot of $H^{-1}(s)G_{dv_s}(s)$ for this system is shown in Fig. 12. The Q factor of the left resonance peak was measured to be 2165 with the right peak having a Q factor of 767. The cantilever Q factor with no applied shunt impedance was measured to be 178. Using the left resonance peak of the shunt controlled cantilever for tapping mode imaging would result in an increase of the effective cantilever Q factor by over 12 times.

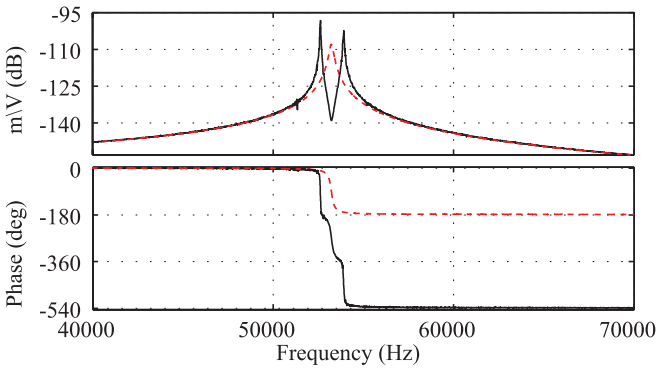

FIG. 12. Frequency response of $G_{dv_s}(s)$ with no active piezoelectric shunt control (- -) and $H^{-1}(s)G_{dv_s}(s)$ with a shunt impedance consisting of an inductance of 313.56 mH and a negative resistance of $-3150\ \Omega$ (—).

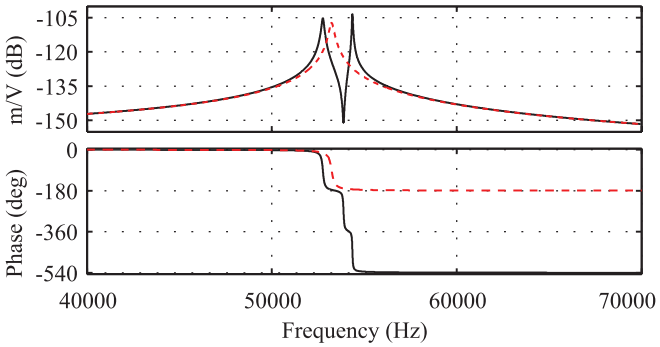

FIG. 13. Frequency response of $G_{dv_s}(s)$ with no active piezoelectric shunt control (- -) and $H^{-1}(s)G_{dv_s}(s)$ with a shunt impedance consisting of an inductance of 306.10 mH and a negative resistance of $-2450\ \Omega$ (—).

V. AFM IMAGING WITH THE ACTIVE PIEZOELECTRIC SHUNT CONTROL TECHNIQUE

To test the efficacy of the active piezoelectric shunt controller images of a sample with fine features were acquired with an NT-MDT NTEGRA AFM.[34] The sample chosen to demonstrate this technique consisted of clusters of gold nanoparticles sputtered on a silicon wafer, which is commercially available from Nanosurf Instruments.[35] The features found on this sample were less than 6 nm high which is ideal for testing the effect of increasing the cantilever Q factor on image quality.

A 350 nm × 350 nm section of the sample was scanned with no cantilever Q factor enhancement at a scan speed of 1 μm/s. The image obtained is shown in Fig. 14(a). The active piezoelectric shunt controller was then placed in the tip oscillation circuit and the cantilever Q factor tuned by varying L and R. The amount of Q enhancement required to improve the quality of the image was determined experimentally. Through trial and error it was found that a Q factor of 410 gave the greatest improvement in image quality. Increasing the Q factor further leads to significant oscillations appearing in the image due to low Z axis feedback loop stability margins. The shunt impedance parameters of $L = 306.10$ mH and $R = -2450\ \Omega$ were required to increase the cantilever Q factor from 178 to 410. A frequency response of $G_{dv_s}(s)$ with active piezoelectric shunt control and $H^{-1}(s)G_{dv_s}(s)$ with the

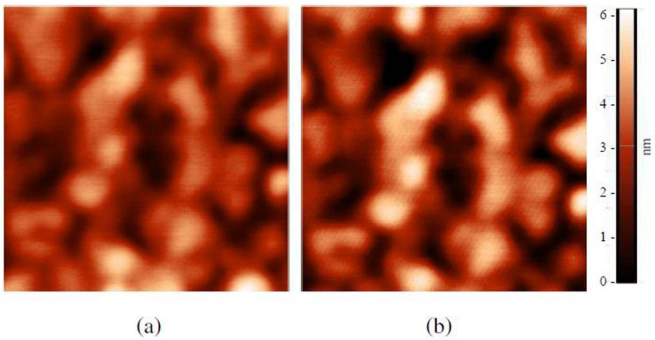

FIG. 14. Images of the gold cluster sample obtained at a scan speed of 1 μm/s with and without enhancement of the cantilever Q factor. The scan area is 350 nm × 350 nm. (a) Q factor 178, no shunt control. (b) Q factor 410, with shunt control.

shunt impedance is shown in Fig. 13. The resonance peak on the left was used for imaging. The image obtained is shown in Fig. 14(b).

Comparing the images of Figs. 14(a) and 14(b) it can be seen that the sample features in the image obtained using active piezoelectric shunt control to enhance the cantilever Q factor are higher, giving a sharper image contrast.

VI. CONCLUSION

The benefits of using a high Q factor cantilever when imaging in tapping mode AFM have been highlighted in this article. The increased force sensitivity and reduced tip-sample force as a result of increasing the cantilever Q factor are beneficial in many imaging applications such as imaging samples with fine features, soft samples, and samples in a fluid environment.

Active piezoelectric shunt control was introduced in this work as a new technique of increasing the Q factor of a piezoelectrically actuated AFM micro-cantilever. This method of Q control has an advantage over existing Q control techniques in that it removes the optical sensor from the Q control feedback loop, reducing measurement noise in the loop. If this method of active Q control is used in conjunction with alternative methods of measuring the cantilever displacement which work by measuring the current through the piezoelectric transducer bonded to the cantilever, the optical sensor may be removed from the instrument altogether. Removing the optical sensor is not only an advantage for reducing sensor noise, it allows for a reduction in the size of the AFM which is a benefit in many applications. The compact size and low cost of the active piezoelectric shunt control instrumentation enables the active piezoelectric shunt controller to be easily integrated into existing AFMs.

A high cantilever Q factor is desired in many other cantilever sensing applications such as measuring air pressure,[30] temperature,[36] humidity,[37] and the concentration of chemical and biological substances.[38–40] The above mentioned benefits of active piezoelectric shunt control are also desirable in these applications.

[1] G. Binnig, C. F. Quate, and C. Gerber, Phys. Rev. Lett. **56**, 930 (1986).
[2] Q. Zhong, D. Inniss, K. Kjoller, and V. Elings, Surf. Sci. **290**, L688 (1993).
[3] G. Meyer and N. M. Amer, Appl. Phys. Lett. **53**, 1045 (1988).
[4] S. Alexander, L. Hellemans, O. Marti, J. Schneir, V. Elings, P. K. Hansma, M. Longmire, and J. Gurley, J. Appl. Phys. **65**, 164 (1989).
[5] F. Gittes and C. F. Schmidt, Eur. Biophys. J. **27**, 75 (1998).
[6] R. D. Jaggi, A. Franco-Obregon, P. Studerus, and K. Ensslin, Appl. Phys. Lett. **79**, 135 (2001).
[7] B. Bhushan, *Springer Handbook of Nanotechnology*, Gale Virtual Reference Library Vol. 2 (Springer, 2006).
[8] T. E. Schaffer, J. P. Cleveland, F. Ohnesorge, D. A. Walters, and P. K. Hansma, J. Appl. Phys. **80**, 3622 (1996).
[9] J. Tamayo, A. D. L. Humphris, R. J. Owen, and M. J. Miles, Biophys. J. **81**, 526 (2001).
[10] B. Anczykowski, J. P. Cleveland, D. Krüger, V. Elings, and H. Fuchs, Appl. Phys. A: Mater. Sci. Process. **66**, S885 (1998).
[11] S. Gao, L. Chi, S. Lenhert, B. Anczykowski, C. M. Niemeyer, M. Adler, and H. Fuchs, ChemPhysChem **2**, 384 (2001).
[12] A. Humphris, A. Round, and M. Miles, Surf. Sci. **491**, 468 (2001).
[13] D. Ebeling, H. Holscher, H. Fuchs, B. Anczykowski, and U. D. Schwarz, Nanotechnology **17**, S221 (2006).
[14] J. Mertz, O. Marti, and J. Mlynek, Appl. Phys. Lett. **62**, 2344 (1993).
[15] M. W. Fairbairn and S. O. R. Moheimani, Rev. Sci. Instrum. **83**, 083708 (2012).
[16] R. Kassies, K. O. van der Werf, M. L. Bennink, and C. Otto, Rev. Sci. Instrum. **75**, 689 (2004).
[17] S. C. Minne, G. Yaralioglu, S. R. Manalis, J. D. Adams, J. Zesch, A. Atalar, and C. F. Quate, Appl. Phys. Lett. **72**, 2340 (1998).
[18] R. Mukhopadhyay, Anal. Chem. **77**, 166A (2005).
[19] A. Pantazi, A. Sebastian, T. A. Antonakopoulos, P. Bächtold, A. R. Bonaccio, J. Bonan, G. Cherubini, M. Despont, R. A. DiPietro, U. Drechsler, U. Dürig, B. Gotsmann, W. Häberle, C. Hagleitner, J. L. Hedrick, D. Jubin, A. Knoll, M. A. Lantz, J. Pentarakis, H. Pozidis, R. C. Pratt, H. Rothuizen, R. Stutz, M. Varsamou, D. Wiesmann, and E. Eleftheriou, IBM J. Res. Dev. **52**, 493 (2008).
[20] B. Rogers, L. Manning, T. Sulchek, and J. Adams, Ultramicroscopy **100**, 267 (2004).
[21] J. Adams, L. Manning, B. Rogers, M. Jones, and S. Minne, Sens. Actuators, A **121**, 262 (2005).
[22] J. Zhao, T. Guo, L. Ma, X. Fu, and X. Hu, Sens. Actuators, A **167**, 267 (2011).
[23] S. O. R. Moheimani, IEEE Trans. Control Syst. Technol. **11**, 482 (2003).
[24] J. Aldrich, N. Hagood, A. von Flotow, and D. Vos, Proc. SPIE **1917**, 692–705 (1993).
[25] F. Bachmann, R. de Oliveira, A. Sigg, V. Schnyder, T. Delpero, R. Jaehne, A. Bergamini, V. Michaud, and P. Ermanni, Smart Mater. Struct. **21**, 075027 (2012).
[26] M. W. Fairbairn, S. O. R. Moheimani, and A. J. Fleming, J. Microelectromech. Syst. **20**, 1372 (2011).
[27] J. Zhao, X. Wang, and J. Tang, J. Vibr. Acoust. **133**, 041009 (2011).
[28] See http://www.brukerafmprobes.com/p-3252-dmasp.aspx for Bruker AFM probes, 2012.
[29] V. Mortet, R. Petersen, K. Haenen, and M. D'Olieslaeger, in *Ultrasonics IEEE Symposium, 2005* (IEEE, 2005), Vol. 3, pp. 1456–1459.
[30] V. Mortet, R. Petersen, K. Haenen, and M. D'Olieslaeger, Appl. Phys. Lett. **88**, 133511 (2006).
[31] P. Sanz, J. Hernando, J. Vazquez, and J. L. Sanchez-Rojas, J. Micromech. Microeng. **17**, 931 (2007).
[32] A. J. Fleming, S. Behrens, and S. O. R. Moheimani, Electron. Lett. **36**, 1525 (2000).
[33] See http://www.linear.com for Linear technology, 2012.
[34] See http://www.ntmdt.com for NT-MDT, 2012.
[35] See http://www.nanosurf.com/ for Nanosurf Instruments, 2012.
[36] A. Boisen, J. Thaysen, H. Jensenius, and O. Hansen, Ultramicroscopy **82**, 11 (2000).
[37] T. Boltshauser, M. Schonholzer, O. Brand, and H. Baltes, J. Micromech. Microeng. **2**, 205 (1992).
[38] H. Lang, M. Baller, R. Berger, C. Gerber, J. Gimzewski, F. Battiston, P. Fornaro, J. Ramseyer, E. Meyer, and H. Güntherodt, Anal. Chim. Acta **393**, 59 (1999).
[39] N. V. Lavrik, M. J. Sepaniak, and P. G. Datskos, Rev. Sci. Instrum. **75**, 2229 (2004).
[40] Y. Lee, G. Lim, and W. Moon, Sens. Actuators, A **130–131**, 105 (2006).